Simultaneous UV and X-ray Spectroscopy of the Seyfert 1 Galaxy NGC 5548. I. Physical Conditions in the UV Absorbers[1]

D.M. Crenshaw[2,3], S.B. Kraemer[4], J.R. Gabel[4], J.S. Kaastra[5], K.C. Steenbrugge[5], A.C. Brinkman[5], J.P. Dunn [2], I.M. George[6,7], D.A. Liedahl[8], F.B.S. Paerels[9], T.J. Turner[6,7], and T. Yaqoob[7,10]

ABSTRACT

We present new UV spectra of the nucleus of the Seyfert 1 galaxy NGC 5548, which we obtained with the Space Telescope Imaging Spectrograph at high spectral resolution, in conjunction with simultaneous *Chandra X-ray Observatory* spectra. Taking advantage of the low UV continuum and broad emission-line fluxes, we have determined that the deepest UV absorption component covers at least a portion of the inner, high-ionization narrow-line region (NLR). We find nonunity covering factors in the cores of several kinematic components, which increase the column density measurements of N V and C IV by factors of 1.2 to 1.9 over the full-covering case; however, the revised columns have only a minor effect on the parameters derived from our photoionization models. For the first

[1]Based on observations made with the NASA/ESA Hubble Space Telescope, obtained at the Space Telescope Science Institute, which is operated by the Association of Universities for Research in Astronomy, Inc., under NASA contract NAS 5-26555. These observations are associated with proposal 9279.

[2]Department of Physics and Astronomy, Georgia State University, Astronomy Offices, One Park Place South SE, Suite 700, Atlanta, GA 30303

[3]crenshaw@chara.gsu.edu

[4]Catholic University of America and Laboratory for Astronomy and Solar Physics, NASA's Goddard Space Flight Center, Code 681, Greenbelt, MD 20771

[5]SRON National Institute for Space Research Sorbonnelaan 2, 3584 CA Utrecht, The Netherlands

[6]Joint Center for Astrophysics, University of Maryland, Baltimore County, 1000 Hilltop Circle, Baltimore, MD 21250

[7]Laboratory for High Energy Astrophysics, Code 660, NASA's Goddard Space Flight Center, Greenbelt, MD 20771

[8]Physics Department, Lawrence Livermore National Laboratory, PO Box 808, L-41, Livermore, CA 94550

[9]Columbia Astrophysics Laboratory, Columbia University, 538 W. 120th Street, New York, NY 10027

[10]Department of Physics and Astronomy, Johns Hopkins University, Baltimore, MD 21218

time, we have simultaneous N V and C IV columns for component 1 (at -1040 km s^{-1}), and find that this component *cannot* be an X-ray warm absorber, contrary to our previous claim based on nonsimultaneous observations. We find that models of the absorbers based on solar abundances severely overpredict the O VI columns previously obtained with the *Far Ultraviolet Spectrograph,* and present arguments that this is not likely due to variability. However, models that include either enhanced nitrogen (twice solar) or dust, with strong depletion of carbon in either case, are successful in matching all of the observed ionic columns. These models result in substantially lower ionization parameters and total column densities compared to dust-free solar-abundance models, and produce little O VII or O VIII, indicating that none of the UV absorbers are X-ray warm absorbers.

Subject headings: galaxies: Seyfert - ultraviolet

1. Introduction

Mass outflow in the form of UV and X-ray absorbers has been shown to be a common phenomenon in the active nuclei of Seyfert galaxies (Reynolds 1997; George et al. 1998; Crenshaw et al. 1999). With the advent of the Space Telescope Imaging Spectrograph (STIS) on the *Hubble Space Telescope* (*HST*), the *Far Ultraviolet Spectroscopic Explorer* (*FUSE*), and the *Chandra X-ray Observatory* (*CXO*), it has become possible to study the absorption systems at unprecedented spectral resolution. Early studies with these instruments (e.g., Crenshaw & Kraemer 1999; Kaastra et al. 2000; Kaspi et al. 2000, 2002; Kriss et al. 2000) proved successful in isolating kinematic components of the absorption and constraining the physical conditions in the gas. The absorbers are often variable in their ionic column densities, and it was quickly realized that simultaneous UV, far-UV, and X-ray observations provide the most valuable information, since they cover an enormous range in ionization, as well as address the uncertain relationship between the UV and X-ray absorbers. Such observations in at least two of the three above wave bands are available for NGC 4051 (Collinge et al. 2001), NGC 3783 (Kaspi et al. 2002; Gabel et al. 2003), NGC 3516 (Kraemer et al. 2002; Netzer et al. 2002), and Mrk 509 (Kraemer et al. 2003; Yaqoob et al. 2003).

In Crenshaw & Kraemer (1999, hereafter CK99), we presented the first STIS echelle observations of the Seyfert 1 galaxy NGC 5548. We confirmed the presence of five kinematic components of absorption in Lyα, N V, and C IV at significant blueshifts with respect to

the systemic velocity, which were first detected in Goddard High Resolution Spectrograph (GHRS) observations (Crenshaw et al. 1999; Mathur et al. 1999). Compared to the GHRS spectra, the column densities of N V and C IV in the STIS spectra had decreased substantially in components 1 and 3 (at respective radial velocities of -1040 and -530 km s^{-1}, relative to an adopted systemic redshift of 0.01676 [CK99]). We attributed these variations to changes in the total column densities of these components, but could not rule out variable ionization for component 1.

In CK99, we calculated photoionization models for the UV absorption components. Based on the C IV and N V column densities from the STIS 1998 data, we found that the ionization parameters and total (ionized plus neutral) hydrogen column densities of components 2 – 5 were too low to produce significant O VII and O VIII columns. Since we only had an upper limit for the C IV column density in component 1 from the STIS 1998 spectrum, we relied on the nonsimultaneous GHRS observations of C IV and N V to produce a model for this component. In this case, the column density ratio of N V/C IV was $\sim$18, which together with the actual columns yielded a high ionization parameter (U = 2.4), as well as the observed O VII and O VIII column densities from earlier observations by *ASCA* (Reynolds 1997; George et al. 1998). On this basis, we suggested that component 1 was likely to be the X-ray warm absorber, with the caveat that none of the UV or X-ray observations were simultaneous. In our conclusions (CK99), we noted that the GHRS C IV and N V observations were obtained $\sim$6 months apart, the *ASCA* observations were $\sim$3 years earlier, and that our findings needed to be checked with simultaneous UV and X-ray observations.

Based on the O VI and H I column densities in *FUSE* observations of NGC 5548, Brotherton et al. (2002) found that component 1 could not be an X-ray warm absorber, and suggested that our original claim could be due in fact to nonsimultaneous observations. Arav et al. (2002) examined the GHRS and STIS spectra, and suggested that our C IV column densities for component 4 were underestimated by a factor $\geq$ 4, due to covering factor effects. Given the importance of resolving these issues, we obtained simultaneous *HST* STIS and *Chanda* observations of NGC 5548 at significantly longer exposure times than those for previous observations. We present the results on the UV observations in this paper, and the X-ray observations in a companion paper (Steenbrugge et al. 2003, in preparation, hereafter Paper II).

2. Observations

2.1. High-Resolution Observations

We obtained STIS echelle spectra of the nucleus of NGC 5548 through a $0\overset{''}{.}2$ x $0\overset{''}{.}2$ aperture on two consecutive days (2002 January 22, 23). We list the details of these observations and previous high-resolution observations obtained by *HST* in Table 1. The setup of the new observations was identical to that of our first STIS observations of NGC 5548 (CK99), covering the full UV range from 1150 – 3119 Å at a velocity resolution (FWHM) of 7 – 10 km s^{-1}. Table 1 shows we were able to devote a much larger exposure time to the new E140M spectra, which contain all of the previously detected intrinsic absorption lines. We also list the previous GHRS observations of the C IV (Crenshaw et al. 1999; Mathur et al. 1999) and N V (Savage, Sembach, & Lu 1997; Crenshaw et al. 1999) regions obtained on separate occasions; we have reanalyzed these spectra for this paper.

We reduced the STIS spectra using the IDL software developed at NASA's Goddard Space Flight Center for the STIS Instrument Definition Team. The data reduction includes a procedure to remove the background light from each order using a scattered light model devised by Lindler (1998). The individual orders in each echelle spectrum were spliced together in the regions of overlap. We found no evidence for variability in the E140M spectra obtained on consecutive days, so we averaged these spectra together for further analysis.

2.2. Low-Resolution Observations and the UV Light Curve

To place the new spectra into context, we have retrieved all of the previous low-resolution spectra of NGC 5548 that contain the 1360 Å continuum region, which are those obtained by the *International Ultraviolet Explorer* (*IUE*), *the Hopkins Ultraviolet Telescope* (*HUT*), and the Faint Object Spectrograph (FOS) on *HST*. We give a brief log of these observations in Table 2.

We retrieved the most recently processed versions of these spectra from the Multimission Archive at the Space Telescope Science Institute (MAST), except for those obtained during the *HST* FOS monitoring on 1993 April 19 – May 27, for which we used the reprocessed versions in Korista et al. (1995). We measured continuum fluxes by averaging the points in a bin centered at 1360 Å (observed frame) with a width of 30 Å, and determined the one-sigma flux errors from the standard deviations. For the *IUE* spectra, this method overestimates the errors (Clavel et al. 1991), and we therefore scaled them by a factor of 0.5 to ensure that observations taken on the same day agree to within the errors on average.

Figure 1 shows the UV continuum light curve of NGC 5548, which spans a 24-year time period. The variations are dramatic, but undersampled, except for the 1988/1989 *IUE* campaign around JD 2,447,600 (Clavel et al. 1991) and the 1993 *HST* FOS/ *IUE* campaign around 2,449,100 (Korista et al. 1995). The last two observations in Figure 1 are from STIS, and demonstrate that the large amplitude variations in the UV have continued. Our previous STIS observation was obtained at a high continuum state [$F_\lambda(1360) = 6.61$ (±0.31) x 10^{-14} ergs s^{-1} cm^{-2} Å^{-1}], whereas the most recent one was obtained at a low state [$F_\lambda(1360) = 1.97$ (±0.20) x 10^{-14} ergs s^{-1} cm^{-2} Å^{-1}]. For comparison, the all-time low occurred on 1992 July 5 (JD 2,448,809) at a flux level of $F_\lambda(1360) = 1.07$ (±0.17) x 10^{-14} ergs s^{-1} cm^{-2} Å^{-1} (Crenshaw, Boggess, & Wu 1993), a factor of ~2 lower than our STIS 2002 observation.

The GHRS fluxes in Figure 1 are estimates, since the continuum regions surrounding the broad emission lines were not observed, due to the small wavelength coverage. In these cases, we used separate fits to the continua and broad emission lines from the STIS spectra, and tried different linear combinations of these fits until we obtained an accurate match to the observed GHRS spectra. The inferred continuum levels for the two GHRS spectra are quite different: $F_\lambda(1360) = 2.7$ (±0.4) x 10^{-14} and 5.6 (±0.4) x 10^{-14} ergs s^{-1} cm^{-2} Å^{-1} for the spectra of the N V and C IV regions, respectively. This has significant ramifications, since we assumed in our original modeling of the intrinsic absorption (CK99) that the GHRS spectra were obtained in a similar state. We will discuss the implications of this result in subsequent sections.

We have also retrieved the *Far-Ultraviolet Spectroscopic Explorer* spectrum of NGC 5548, covering the range 905 – 1187 Å, which was obtained on 2000 June 7 (JD 2,451,703) by Brotherton et al. (2002). The continuum level at this time was even lower than that of the STIS 2002 spectrum. In the region of overlap, the STIS 2002 spectrum has a continuum flux that is 1.5 times that of the *FUSE* spectrum. In these low continuum states, the broad emission-line fluxes are also low, and due to the resulting contrast, the contributions of the narrow-line region (NLR) to the emission-line profiles is much easier to determine. In particular, the narrow components of O VI $\lambda\lambda1031.9$, 1037.6 were identified in the *FUSE* spectrum by Brotherton et al. (2002), and the narrow components of Lyα λ 1215.7, C IV $\lambda\lambda1548.2$, 1550.8, and C III] $\lambda1908.7$ were previously identified and measured in the low-state FOS spectrum by Crenshaw et al. (1993), and are also easily detected in the STIS 2002 spectra.

2.3. Absorption-Line Variations

In Figure 2, we show the C IV profile from the three high-resolution spectra of this region, and label the kinematic components identified in our previous papers (Crenshaw et al. 1999; CK99). All of the previously identified components are still present in the new spectrum, but the strengths of some components have changed. As noted in CK99, absorption components 1 and 3 showed evidence for a significant decrease in their C IV and N V columns between the GHRS 1996 and STIS 1998 observations (although we could only place an upper limit on the C IV column for component 1 in the STIS 1998 data); the other components were consistent with no change. This trend has continued $\sim$4 years later; components 1 and 3 are still highly variable, with substantial *increases* in the C IV and N V columns since the STIS 1998 observation (for N V, compare Figure 3 with plots in our earlier papers). Thus, the pattern for components 1 and 3 has been an increase in ionic column densities with decreasing continuum flux. However, there are only three observations of each ion, and this does not prove a direct connection between column changes and variations in the ionizing flux (see §4.5).

Figure 3 shows a plot of the STIS 2002 data in the regions where intrinsic absorption is detected. As in the past, absorption is detected in the lines of Lyα λ 1215.7, N V $\lambda\lambda$ 1238.8, 1242.8, and C IV $\lambda\lambda$1548.2, 1550.8. At this low state, and with a higher signal-to-noise spectrum, we have still not detected any absorption components from lower ionization lines, such as Si IV $\lambda\lambda$1393.8, 1402.8 or Mg II $\lambda\lambda$ 2796.3, 3803.5. Component 6, near the systemic velocity, is still only seen in Lyα, and is likely due to the interstellar medium or halo of the host galaxy (CK99). Components 2 and 5 are relatively narrow and uncomplicated. There is considerable structure in components 1, 3, and 4 that has persisted over $\sim$6 years. Components 1 and 4 each show a strong subcomponent in their red wings, and component 3 appears to consist of at least three roughly equally-spaced subcomponents. Figure 2 shows that it is the two subcomponents on either side of the central trough in component 3 that have increased dramatically in strength in the latest STIS spectrum.

2.4. Spectral Fits and Absorption-Line Measurements

The procedures we used to measure the absorption lines follow those of Crenshaw et al. (1999). To determine the shape of the underlying emission, we fit cubic splines separately to the continuum and the emission lines. For the continuum, we fit four wavelength regions unaffected by emission or absorption features spanning the full range of the spectrum. For this low-state spectrum, the broad and narrow emission components are easily distinguished by inflections in the profiles (see also Crenshaw et al. 1993). We therefore performed a

single spline fit to each broad and narrow component of Lyα and C IV, again using segments unaffected by other emission or absorption lines. To fit the N V emission, which is relatively weak and blended with Lyα, we reproduced the C IV broad and narrow profiles at their expected N V positions (assuming the flux ratio of N V $\lambda1238.8/\lambda1242.8 = 2$), and scaled the profiles until a suitable fit was obtained. We note that our philosophy is to use the lowest reasonable emission-line profiles needed to fit the regions surrounding the absorption accurately. To normalize the absorption profiles, we divided the observed spectra by our spline fits. As described in Crenshaw et al. (1999), we determined uncertainties in the absorption parameters from photon statistics and different reasonable placements of the continuum and emission-line profiles.

Figure 3 shows our fits to the spectrum. We also show the narrow emission-line profiles separately, in order to gauge their fluxes above zero as a function of radial velocity. The narrow-line profile of C IV (and likely N V) has a strong blue tail, which is common for Seyfert galaxies (Vrtilek & Carleton 1985), particularly for high-ionization lines from the inner NLR (Kraemer & Crenshaw 2000). The Lyα profile shows a small bump in its red wing – the nature of the bump is uncertain. The centroids of the N V and C IV profiles are shifted to the red, relative to Lyα. This is due to the contribution from the weaker member of the doublets in emission, which is most noticable in N V.

An important aspect of Figure 3 is that it shows that component 4 dips below the narrow emission profiles in all three ions. Arav et al. (2002) find that in the earlier STIS data, their fits to the narrow-line profiles just skim the bottom of the absorption troughs from component 4. These authors suggest that the narrow emission lines are therefore not covered by the absorption components, and that component 4 in particular is likely to be heavily saturated. However, with the advantage of having a low-state spectrum, we find that the fluxes of the narrow-line profiles do exceed the troughs of component 4. Thus, *at least* a portion of the NLR in this small aperture ($0\farcs2$ x $0\farcs2$) is covered by absorption component 4.

Table 3 shows our measurements of the radial velocity centroids, widths (FWHM), and covering factors for each component. The radial velocities, widths, and associated one-sigma uncertainties are based on averages of the unblended components in N V and C IV. A comparison with our results on the previous GHRS and STIS observations (CK99) shows that the velocity centroids have not changed (outside of the uncertainties) over the previous six years. However, the widths of components 1 and 3 have increased substantially since the first STIS observations: from 85 to 222 km s^{-1} for component 1 and from 78 to 159 km s^{-1} for component 3. We attribute these increases in FWHM to increases in the depths of the subcomponents, relative to the central cores. We find that the widths of these components

at the continuum level did *not* change, which supports our conclusion that the increases in FWHM are due to changes in the ionic columns rather than changes in the coverage of velocity space by the components.

In addition to the above measurements, we have taken advantage of the higher signal-to-noise ratio of the STIS 2002 spectrum to determine the covering factors (C_{los}) for the cores of several components. We used the technique of Hamann et al. (1997) for doublets to determine C_{los}, which is the fraction of continuum plus emission that is occulted by the absorber in our line of sight. Since we have no information to the contrary, our measurements implicitly assume that the continuum, broad emission, and narrow emission are equally covered by each absorption component. Figure 2 shows that the only component of absorption in C IV that is not blended with another is component 4. However, for N V, the doublets of 2, 3, and 4 are clean (N Vλ1242.8 component 5 is blended with N Vλ1238.8 component 1, see Crenshaw et al. 1999). Furthermore, the wings of these components are blended with those from other components. Thus, we can only reliably determine covering factors for the cores of components 2, 3, and 4.

Our derived covering factors are given in Table 3. Components 2, 3, and 4 all show nonunity covering factors in their cores; previously, we had only been able to determine that component 4 had a nonunity covering factor (Crenshaw et al. 1999). The actual values in this table are from the N V doublet, whereas the lower limits are from the residual intensities in Lα. These values are consistent with our estimates or lower limits from the previous GHRS and STIS spectra. Gabel et al. (2003) show that it is possible for the total covering factor (i.e., that for continuum plus emission) to differ among different lines (e.g., C IV and N V). This effect arises as a result of different covering factors for the continuum and emission-line regions, combined with different contributions of the continuum and emission-line fluxes to the underlying emission. The only direct test that we have of this effect is for component 4; in this case we find that the covering factors from the C IV doublet is 0.91 ± 0.03, which is the same as that from the N V doublet to within the errors. For components 2 and 3, we must assume that the C IV covering factors are the same as those derived for N V. Since we cannot measure covering factors for components 1 and 5, we assume that $C_{los} = 1$ for these two components. Brotherton et al. (2002) independently derived covering factors for the O VI absorption components, and their values agree with ours to within the uncertainties. In addition, they obtained $C_{los} = 0.98$ (±0.12) and 0.94 (±0.14) for components 1 and 5, respectively, which indicates that our assumption of unity covering factors for these two components is a reasonable one.

To determine the ionic column densities for each component, we converted each normalized profile to optical depth as a function of radial velocity, and integrated across the profile,

as described in Crenshaw et al. (1999). For components 2, 3 and 4, we determined the optical depths using the measured C_{los} values and the formalism of Hamann et al. (1997). For the other components, we assumed $C_{los} = 1$. As we stated in the preceding paragraph, this appears to be a reasonable assumption for components 1 and 5, and a necessary assumption for component 6 if it is indeed due to the interstellar medium or halo of the host galaxy.

We list the ionic column densities for each component in Table 4. For the GHRS and STIS 1998 spectra, we have remeasured the columns for components 2, 3, and 4 assuming the covering factors we determined from the STIS 2002 spectra. We give upper limits to the Si IV absorption, since they provide useful constraints for the photoionization models. We consider the H I column densities from Lα to be lower limits. As mentioned in CK99, the components are more blended in Lyα than those in the other lines and are therefore more heavily saturated. Furthermore, the H I column densities from Lyβ in the FUSE spectrum (Brotherton et al. 2002) are 5 –8 times higher than the values in Table 1. It is unlikely that this could be due to variability of the H I column alone, since we don't see evidence for strong variations in other lines of components 2, 4, and 5. The most straightforward explanation is that the Lyα lines are indeed heavily saturated, and our measurements are lower limits. It would be interesting to obtain a longer *FUSE* exposure to detect higher-order Lyman lines, to check for saturation in Lyβ.

To investigate the effects of the nonunity covering factors on the measured ionic columns, we compared the values in Table 4 with those we determined previously for the GHRS and STIS 1998 data (CK99). This comparison reveals that the remeasured C IV columns are 1.2 to 1.5 times larger than those previously determined assuming $C_{los} = 1$. The effects on the N V measurements are the same or slightly larger; the remeasured N V columns are 1.2 to 1.9 times larger.

Our earlier statements on absorption variability based on the observed spectra are borne out by the measurements in Table 4. Component 1 shows huge (factor of 6 – 10) changes in the N V and C IV column densities, and component 3 shows significant (factor of $\sim$2) variations in both ions. Other components show no evidence or only marginal evidence for column density variations, given the uncertainties.

2.5. Discussion of Observational Results

For the first time, we have direct measurements of the N V and C IV column densities in component 1 from simultaneous observations (the GHRS observations were not simultaneous, and the previous STIS observation could only place a lower limit on the C IV column). Thus,

we are able to check our previous suggestion that component 1 might be the X-ray warm absorber, based on its high N V/C IV ratio (= 18) from the GHRS observations. In Table 4, we see that component 1's N V/C IV ratio in the STIS 2002 spectrum is only 2.5, which is close to the ratios for components 2, 4, and 5. Based on our models (§4), this value does not produce significant O VII or O VIII columns, and component 1 in the STIS 2002 spectrum *cannot* be an X-ray warm absorber at that epoch. Given this finding, we can no longer assume that the GHRS N V/C IV ratio provides an appropriate constraint on the physical conditions in component 1. The ionic column densities in Table 4 are strongly variable over 2 – 4 years, and it is certainly possible that they varied over the six-month interval between the GHRS observations. Furthermore, in §2.2 we showed that the GHRS C IV and N V observations were obtained at different continuum states, so that one cannot call upon a similar ionization state of the gas as a reason for using this ratio. Finally, photoionization models of component 1 using simultaneous observations of the O VI and Lyβ absorption in *FUSE* data (Brotherton et al. 2002) indicate that this component has an ionization parameter too low to be a warm absorber at the epoch of observation (2000 June 7). Thus, there is no longer any significant evidence that component 1 is, or was, a warm absorber. Note that this does not rule out the presence of X-ray absorption from a component of more highly ionized gas at this radial velocity, and in fact, Kaastra et al. (2002) present such evidence based on C VI absorption in *CXO* spectra at the same approximate radial velocity as component 1 (see §4.4). Furthermore, in our simultaneous HETGS spectrum, the high ionization Si XIV Lyα line is dominated by a velocity component compatible with UV component 1 (Paper II).

As noted earlier, Arav et al. (2002) suggest that the narrow emission lines in the STIS aperture are not covered by the absorption components. They conclude that component 4, which has the deepest troughs, is therefore much more saturated than it appears. In particular, they suggest that the C IV column densities for component 4 are at least four times greater than we had previously measured (Crenshaw et al. 1999). However, with the new low-state STIS spectrum, we find that the peaks of the narrow-line profiles do extend above the troughs of component 4 in each line (Lα, C IV, and N V). Thus, *at least* a portion of the NLR is occulted by the UV absorber associated with component 4. As discussed earlier, the inclusion of nonunity covering factors does increase the measured column densities, but only by a factor of 1.2 to 1.9. In particular, the C IV column density for component 4 increased by a factor of only 1.2 with the inclusion of the nonunity covering factor. Thus, we find no evidence for the severe underestimation of column densities suggested by Arav et al. (2002).

There are a couple of caveats that we should mention concerning the above discussion. First, we have implicitly assumed that the continuum source, BLR, and NLR are all covered

by the same fraction, but it could be that only the NLR is partially covered. In the latter case, one could devise emission-line profiles for the uncovered NLR that skim the bottoms of the component 4 troughs, and thereby produce much higher ionic column densities; however, we have no evidence that this is actually the case. Second, we have not been able to accurately determine the variation of covering factor as a function of radial velocity for any component, due to a combination of blending and insufficient signal-to-noise. Thus, the column densities could be higher if the covering factor decreases in the wings. However, we expect this effect would be small, since it seems unlikely that saturation effects in the wings would be as large as those in the troughs, which are not severe. An accurate determination of the covering factor as a function of radial velocity should be possible with a substantially longer exposure time.

For the *FUSE* data, Brotherton et al. (2002) generated fits to the O VI emission profile assuming a "covered NLR" and an "uncovered NLR" case, and prefer the uncovered case. However, it looks to us as though the NLR flux from either fit exceeds the trough of component 4, and the covered NLR is therefore preferable. In addition, the width of their narrow O VI profile is $\sim$400 km s^{-1} for the uncovered case and $\sim$650 km s^{-1} for the covered case; the latter is similar to our values of $\sim$700 km s^{-1} for C IV and 590 km s^{-1} for Lyα. Thus, it appears that the covered case is much more likely for O VI, as well as the other lines. However, we cannot rule out the possibility that some fraction of the narrow O VI emission is not covered, particularly in the large (30″ x 30″) *FUSE* aperture.

In Figure 4, we show the *FUSE* spectrum in the region of the O VI lines. The spectrum was normalized by dividing by the covered NLR fit of Brotherton et al. (2002); each member of the doublet is plotted as a function of radial velocity. The positions of the STIS components align well with the absorption troughs (at most there is a 10 km s^{-1} offset). Brotherton et al. find that there is a velocity offset of $\sim$100 km s^{-1} between the STIS and *FUSE* components, and suggest this offset is probably due to calibration uncertainties. The source of the discrepancy is actually the different systemic redshifts used; Brotherton et al. used the H I 21-cm value of 0.017175, whereas we use the emission-line redshift of 0.01676 to be consistent with our earlier papers, which amounts to a velocity offset of 125 km s^{-1}.

For components 1, 2, 4, and 5, the blue member of the O VI doublet in Figure 4 is clearly deeper than the red member, indicating that these lines are not heavily saturated. However, for component 3 (Brotherton et al.'s components 2.5 plus 3), the two lines lie on top of each other, which suggests heavy saturation in O VI across the profile and a covering factor of $\sim$0.45 (in agreement with Brotherton et al.'s value for component 2.5). We suggest that the O VI absorption profile for component 3 is heavily saturated, and should therefore be considered a lower limit. The inferred large O VI column is consistent with the high

N V/C IV ratio (= 9.2) that we find for component 3, as discussed in §4.2 and §4.3.

3. Photoionization Models of the UV Absorbers

Photoionization models for this study were generated using the code CLOUDY90 (Ferland et al. 1998). We have modeled the absorbers as matter-bounded slabs of atomic gas, irradiated by the ionizing continuum radiation emitted by the central source. As per convention, the models are parameterized in terms of the ionization parameter, U, the ratio of the density of photons with energies $\geq$ 13.6 eV to the number density of hydrogen atoms at the illuminated face of the slab, and the total hydrogen column density, N_H (= N_{HI} + N_{HII}). For $n_H \lesssim 10^8$ cm^{-3}, the predicted ionic columns densities are not sensitive to density. For the models, we have assumed only thermal broadening, since 1) the absorption line widths could be due to the superposition of unresolved kinematic components and 2) comparison models assuming turbulent velocities of $\leq$ 300 km s^{-1} predict nearly identical ionic columns. The models were deemed successful when the predicted N V and C IV column densities matched those observed to within the measurement errors.

For the spectral energy distribution (SED) of the ionizing radiation, we used the X-ray continuum given in Paper II. After correcting for Galactic reddening (E_{B-V} = 0.03) and intrinsic reddening (E_{B-V} = 0.04, see Kraemer et al. 1998), we fit the UV continuum fluxes from 1170 to 3000 Å with a power law of index $\alpha_\nu \approx -1.0$. We assumed that the UV continuum turns over at the Lyman limit, with $\alpha_\nu = -1.4$, joining the the EUV and X-ray continua at ~100 Å (124 eV). Figure 5 shows our adopted SED, which is similar to that used in CK99; tests show that the two SEDs yield essentially identical results.

4. Model Results

We use our simultaneous observations of N V and C IV as the principal constraints on the models. Additional simultaneous lower limits on H I (from Lyα) and upper limits on Si IV are also helpful. Since the GHRS C IV and N V observations were not simultaneous and were, in fact, obtained during different continuum states, we do not calculate models for the GHRS data, but use the observed columns to investigate the absorption variability. For additional constraints, we make use of the simultaneous *CXO* observations, as well as the nonsimultaneous observations with *FUSE*, keeping in mind that the ionic column densities are almost certainly variable. For models of the STIS columns, we begin with the most well-constrained data, which are those from the 2002 observation.

4.1. Dust-Free, Solar-Abundance Models of the STIS 2002 Data

For the STIS 2002 data, we initially assumed that the UV absorbing gas was free of cosmic dust. We also assumed solar elemental abundances (see Grevesse & Anders 1989), which are, by number relative to H, as follows: He = 0.1, C = 3.4 x 10^{-4}, N = 1.2 x 10^{-4}, O = 6.8 x 10^{-4}, Ne = 1.1 x 10^{-4}, Mg = 3.3 x 10^{-5}, Si = 3.1 x 10^{-5}, S = 1.5 x 10^{-5}, and Fe = 4.0 x 10^{-5}.

The resulting parameters from our best fitting models are listed in Table 5 (each designated as component number followed by "solar"), while the predicted ionic column densities are given in Table 6, along with the observed values for comparison. For each component, we matched the observed column densities N_{CIV} and N_{NV} to well within the measurement errors. In each case, the model predictions for N_{HI} exceeded the lower limits determined from Lyα and the predictions for N_{SiIV} are $<< 10^{12}$ cm^{-2} (lower than the observational upper limits).

As mentioned previously, we have been able to determine simultaneous N V and C IV columns for component 1 for the first time. The derived ionization parameter and column density for component 1 are lower than those from CK99 by factors of ~13 and ~200, respectively, and the predicted O VII and O VIII column densities are undetectable. This supports our conclusion (§2.5) and that of Brotherton et al. (2002) that the gas responsible for the UV absorption in component 1 cannot produce the observed X-ray absorption. Again, this does not exclude the presence of more highly ionized gas at the same velocity.

Table 6 also lists the observed columns of H I and O VI from the *FUSE* spectrum (Brotherton et al. 2002) obtained ~19 months earlier. Based on similar velocity coverages, we have added their components 0.5 and 1 together for our component 1, and combined their components 2.5 and 3 for our component 3. As noted previously, we use the O VI value for component 3 as a lower limit. Although we were able to obtain good fits to the N V and C IV columns and a reasonable match to the H I columns (except for component 3), the dust-free models predict O VI columns far in excess of those measured, by similar factors of 6 – 8. This discrepancy cannot be due to the ionizing continuum used in the model since, unless there is extreme structure in the ionizing continuum in the vicinity of the O V (113.9 eV) and O VI (138.1eV) threshold energies, the model predictions for N_{OVI} do not depend strongly on SED. We consider it highly unlikely that variability could be the main source of the O VI discrepancies, for the following reasons. 1) None of the other ions show significant variability in components 2, 4, and 5. 2) The *FUSE* spectrum was in a lower continuum state than that for the STIS 2002 spectrum, which would result in even higher predicted O VI columns for components 1 and 3, according to our models. 3) It seems very unlikely that the observed O VI columns would all be low by roughly the same amount as a result of

extreme decreases in the total column density for each component during this epoch.

Thus, it seems reasonable that these models severely overpredict the O VI columns, even though the observations are not simultaneous. Brotherton et al. (2002) suggested that models based on N_{NV}/N_{CIV} alone may be unreliable due to super-solar nitrogen abundances. We investigate this possibility in the next section and the possibility that the discrepancies can be explained by depletion (primarily of carbon) into dust grains in §4.3.

4.2. Nitrogen-Enhanced Models of the STIS 2002 Data

We generated a second set of models with a nitrogen abundance that is two times solar, and assumed that the enhanced nitrogen is at the expense of carbon alone. This is the simplest reasonable adjustment of elemental abundances that can be made, for the following reason. If enrichment of the interstellar medium above solar abundances is due to intermediate-mass stars, the carbon gets converted to nitrogen first through the CNO process, whereas the oxygen goes to nitrogen at later times and higher temperatures (Maeder & Meynet 1989). Thus, for these models, we keep the same abundances as before, except that $C = 2.2 \times 10^{-4}$ and $N = 2.4 \times 10^{-4}$ by number relative to H.

The model results are listed in Tables 5 and 6 under the designation "2xN". We were able to match the observed N V and C IV columns as before to well within the measurement errors (and N_{SiIV} is $<< 10^{12}$ cm^{-2} in all cases). Furthermore, we have obtained a reasonable (within a factor of two) match to the N_{OVI} for components 1, 2, 4, and 5, as well as a value for component 3 that is consistent with the lower limit. In addition, the predicted H I column for component 3 is much closer to the observed value from *FUSE*. As can be seen in Table 5, the principal effect of enhancing nitrogen and depleting carbon is that the ionization parameter and column density of each component must be lowered substantially to match the observed N V/C IV ratio and their columns.

The values for U and N_H are now in approximate agreement with those determined by Brotherton et al. (2002), except for component 3. Based on the high N_{NV}/N_{CIV} ratio (= 9.2) for component 3, we determined a much larger column density and ionization parameter than did Brotherton et al. (2002), and our prediction for N_{OVI} is ~8 times greater than their estimate. However, given evidence that the O VI absorption is heavily saturated and the quoted column density is a lower limit, our prediction is consistent with the observations. Thus, for all of the components, the enhanced nitrogen models provide a reasonably good match to all of the ionic columns.

4.3. Dusty Solar Models of the STIS 2002 Data

We generated a third set of models that starts with solar abundances, but includes dust within the UV absorbers. We assumed the following depletions from solar-abundance gas phase (see Snow & Witt 1996): C, 65%; O, 25%; Mg, 80%; Si, 94%; and Fe, 95% (N is not depleted). The results are listed in Tables 5 and 6 under the designation "dusty". Again, we were able to match the observed N V and C IV columns, the N_{OVI} for components 1, 2, 4, and 5, and the lower limit to N_{OVI} in component 3. The predicted H I columns are also close to the *FUSE* values. Thus, the dusty UV models provide an equally good match to the ionic columns as those provided by the enhanced nitrogen models. The ionization parameters are nearly identical for the two cases, whereas the N_H columns for the dusty models are 2 – 3 times those of the enhanced nitrogen models.

As noted above, in Kraemer et al. (1998) we estimated an intrinsic reddening of the NLR in NGC 5548 of $E_{B-V} \approx 0.04$ mag. Assuming a Galactic ratio of reddening to the total hydrogen column (see Shull & van Steenberg 1985), this corresponds to a total hydrogen column density of 2.1×10^{20} cm^{-2}. This in remarkable agreement with our total model hydrogen column of 2.3×10^{20} cm^{-2}. Hence, it is possible that the reddening of the continuum and emission lines occurs in the same gas in which the UV absorption lines arise. Kraemer et al. (1998) place the high-ionization inner NLR at a distance of ~ 1 pc from the central source, which is comfortably outside the dust sublimation radius (r_{sub}). Following Barvainis (1987), and assuming a dust sublimation temperature of 1500 K (Salpeter 1997), $r_{sub} = 1.3 \times L_{46}^{1/2}$, where L_{46} is the UV – X-ray luminosity of the central source in units of 10^{46} erg s^{-1}. Based on our continuum fit, $L_{46} \approx 0.01$, and hence $r_{sub} \sim 0.13$ pc, which is well inside the inner NLR and the majority of the UV absorbing gas.

4.4. Constraints from X-ray Spectra

From our contemporaneous *CXO* LETGS spectrum (see Paper II), we determined an O VI column density of 2×10^{16} cm^{-2} from the absorption lines at 21.79 Å and 22.01 Å. We predict a total $N_{OVI} = 1.1 \times 10^{16}$ cm^{-2} for the nitrogen-enhanced models and 1.8×10^{16} cm^{-2} for the dusty models, mostly from component 3, which are close to the LETGS value. This suggests that at least half of the observed O VI column comes from the absorbers detected in the UV. Notably, Brotherton et al. (2002) derive a total $N_{OVI} \approx 4.1 \times 10^{15}$ cm^{-2}, significantly below the LETGS-derived value, which we suggest is further evidence that the O VI lines in component 3 are saturated. Regarding the "classic" warm absorbers, the total O VII and O VIII columns from the contemporaneous *CXO* spectrum are 5×10^{17} cm^{-2} and 1.5×10^{18} cm^{-2}, respectively. The UV components do not make significant contributions to

the O VII ($<$ 15%) and O VIII ($<$ 1%) columns, confirming the presence of more highly ionized gas than found in the UV.

In Kaastra et al. (2002), the C VI Lyα line detected in the 1999 LETGS spectrum was fitted using a sum of narrow components at the velocities of the five UV absorbers. The C VI profile in our contemporaneous LETGS spectrum shows less structure (see Paper II), and it was best fit with three velocity components at -1050 km s^{-1}, -520 km s^{-1}, and -160 km s^{-1}. The combined C VI column density from these components is 1.4 x 10^{17} cm^{-2}. Based on our dusty UV models, only component 3 possesses a significant C VI column (7.4 x 10^{15} cm^{-2} for the nitrogen-enhanced model, 1.3 x 10^{16} cm^{-2} for the dusty model), and thus the UV components contribute $<$10% of the observed C VI. Since C VI requires a substantially higher ionization potential for its creation than O VI (392.1 eV and 113.9 eV, respectively), this is an indication of more highly ionized gas *at the radial velocities of the UV absorbers*, as also seen in NGC 3783 (Kaspi et al. 2002) and Mrk 509 (Yaqoob et al. 2003; Kraemer et al. 2003).

4.5. Changes in the Absorbers

As noted previously, components 1 and 3 show strong variations in their ionic columns, whereas the other components show little evidence for variations. As in CK99, we can ask if the ionic column variations can be attributed to either variable ionization or variable total column (e.g., from bulk motion of gas across the line of sight). As shown in Figure 1, different UV continuum flux levels were observed in the four high-resolution spectra of NGC 5548, with the GHRS CIV and STIS 1998 spectra taken during relatively high states and the GHRS N V and STIS 2002 spectra taken during low states. If the absorbers respond to changes in the ionizing continuum, we would expect both *smaller* N V and C IV columns and *larger* N_{NV}/N_{CIV} ratios during high flux states. This is clearly not the case for component 3; although the columns are smaller in 1998 compared to 2002, the N V/C IV ratio is smaller as well (6.8 in 1998 compared to 9.2 in 2002). Although we only have an upper limit for N_{CIV} in the STIS 1998 data for component 1, N_{NV} requires an ionizing continuum a factor of $\sim$6 higher during the STIS 1998 observations. However, the observed UV flux was only 3.4 times as bright. Hence, either the amplitude of the variations in the EUV ionizing radiation is about twice as large as that in the UV, or the observed changes in the ionic columns for component 1 are not consistent with the changes in the continuum flux.

Given the lack of response of the absorbers to changes in the continuum flux (with the possible exception of component 1) we can derive upper limits to their electron densities and lower limits to their distances from the central continuum source. The timescale for

the recombination of an ion X_i is given by the following expression (Krolik & Kriss 1995; Bottorff, Korista, & Shlosman 2001):

$$t(X_i) = \left[\alpha(X_i) \, n_e \, \left(\frac{f(X_{i+1})}{f(X_i)} - \frac{\alpha(X_{i-1})}{\alpha(X_i)} \right) \right]^{-1}, \tag{1}$$

where $\alpha(X_i)$ is the recombination coefficient for ion X_i, $f(X_i)$ is the fraction of element X in ionization state i, and n_e is the electron density. Based on our model predictions, components 1, 2, 4, and 5 have similar conditions, with $T \approx 2.4 \times 10^4$ K, $f(C\ V)/f(C\ IV) \approx 6$, and $f(N\ VI)/f(N\ V) \approx 1.3$. For component 3, which is at higher ionization, we predict $T \approx 4.3 \times 10^4$ K, $f(C\ V)/f(C\ IV) \approx 70$, and $f(N\ VI)/f(N\ V) \approx 16$. Assuming only radiative recombination (see Shull & van Steenberg 1982), and a timescale of $\gtrsim 4$ yrs (the interval between STIS observations), we obtain the following upper limits on electron density: for Component 3, 15 cm^{-3} and 50 cm^{-3} (from C IV and N V, respectively); for the lower ionization components, we obtain 150 cm^{-3} and 650 cm^{-3}. Based on our estimate of the central source luminosity above the Lyman limit (see Kraemer et al. 1998) and our ionization parameters, the lower limit to the radial distances of the low ionization components is between 20 and 250 pc, while that for component 3 is between 150 and 250 pc from the central source. These constraints place the absorbers at large enough distances that they may cover much of the entire NLR. However, we note that the continuum and absorption variations are obviously not well characterized, with just a few high-resolution observations widely separated in time. Since the ionic columns for components 2, 4, and 5 have not varied significantly, despite large variations in the continuum fluxes, the above constraints are likely valid. For the variable components 1 and 3, however, we cannot rule out changes in ionization in response to unobserved continuum variations on time scales smaller than years. Thus, we consider the limits on the densities and radial locations of components 1 and 3 to be loose constraints; more frequent monitoring at high spectral resolution are needed to test them.

Since there is no clear signature of a response to the changes in the continuum flux, we can investigate whether or not the variations in ionic column densities are consistent with changes in the total column densities of the absorbers. Pursuing this, we generated sets of nitrogen-enhanced and dusty models for components 2 – 5 in the STIS 1998 data, with the same ionization parameters used for the STIS 2002 models, but adjusting the total column densities (see Table 7). In each case, the predictions for N_{CIV} and N_{NV} match the measured values to within the measurement errors. Components 2, 4, and 5 show only small changes in the total columns, consistent with our earlier claims of no or marginal variability of these components. Component 3 shows a much smaller column in the 1998 data, and the agreement between observed and predicted columns indicates that the variations are likely dominated by changes in the total column (by a factor of $\sim$2.6). We did not attempt to model component 1, since we only had an upper limit for N_{CIV} from the STIS 1998 spectra.

Of course, we can reproduce the observed N V column in 1998 by reducing the total column of gas by a factor of $\sim$6. Obviously, the larger C IV and N V columns in components 1 and 3 for the two GHRS observations (compared to the STIS 1998 values) could also be attributed to changes in the total columns, but we have no constraints on possible ionization changes.

5. Summary

New *HST* STIS echelle spectra, combined with simultaneous *CXO* observations, place tighter constraints on the UV absorbers of NGC 5548 than were possible in the past. Simultaneous detection and measurement of the C IV and N V absorption lines in component 1 show that this component is *not* an X-ray warm absorber, in agreement with the conclusion of Brotherton et al. (2002) based on *FUSE* observations of O VI and Lyβ, and despite our earlier claim based on nonsimultaneous GHRS observations (CK99). The new STIS observations were obtained when the UV continuum and broad emission lines fluxes were low, allowing us to easily distinguish the narrow components of the emission lines. We present direct evidence that UV absorption component 4 covers at least a portion of the NLR. Our derivation of the covering factors indicates that our previous C IV and N V column densities were underestimated by factors of 1.2 – 1.9, and not the >4 factors suggested by Arav et al. (2002).

Our dust-free, solar-abundance models of the UV absorbers in the STIS 2002 data match the C IV and N V columns well, but they severely overpredict the observed O VI columns in the nonsimultaneous *FUSE* data. Models that include enhanced nitrogen or elemental depletion into dust, in both cases reducing the carbon in gas phase, provide reasonable (within a factor of two) matches to the O VI columns. Absorption lines (or lack thereof) from heavier refractory elements that tend to be depleted into dust (e.g., Fe, Mg, Si), would be extremely useful for discriminating between these two models, but unfortunately there are no suitable high-ionization lines from these elements in the UV. In particular, Si IV, with a creation ionization potential of 33.5 eV, has an insignificant column even in our dust-free models.

If the dusty models are correct, then the total hydrogen column from the absorbers is exactly the amount needed to redden the inner NLR by the observed amount, E(B−V) = 0.04 (Kraemer et al. 1998), assuming a Galactic dust-to-gas ratio. This is a piece of evidence in favor of the dusty models, although it is possible that the NLR clouds provide their own reddening. There is strong evidence for dust in UV absorbers at distances of $\gtrsim$ 100 pc in NGC 3227 (Crenshaw et al. 2001) and Akn 564 (Crenshaw et al. 2002). However, in these cases, the absorbers appear at radial velocities close to systemic and are probably due to the

host galaxy, as opposed to the outflowing absorbers seen in NGC 5548.

Our absorber models indicate that none of the UV components contribute significantly to the O VII and O VIII columns seen in the X-rays, in agreement with the conclusions of Brotherton et al. (2002). Hence, none of the UV absorbers is a classic X-ray warm absorber. However, the UV components, particularly the higher ionization component 3, do contribute $>50\%$ of the O VI column and $5 - 10\%$ of the C VI column measured in the *CXO* spectra (Paper II).

Regarding the source of the ionic column variations in components 1 and 3, we come to the same conclusions as in CK99. The variations in component 3 are dominated by changes in the total column density, whereas those in component 1 are probably dominated by column changes, although we cannot rule out variable ionization of the gas for this component. As discussed in CK99, changes in total column due to bulk motion of the gas across our line of sight in NGC 5548 require transverse velocities of ~ 1500 km s^{-1}.

There are a couple of indications that the UV components 2, 4, and 5 are at significant distances from the active nucleus of NGC 5548. We have presented direct evidence that component 4 covers at least a portion of the high-ionization, inner NLR, at a distance of ~ 1 pc from the central continuum source (Kraemer et al 1998). Also, these absorbers apparently do not respond to continuum variations over time scales of years, which suggests that they are at distances between 20 and 250 pc from the nucleus.

Desirable observations in the future include coordinated UV and FUV observations at high spectral resolution, to check our conclusions on the nonsolar abundances in the gas phase of the absorbers. Longer exposure times on the above would be desirable, to derive covering factors as a function of radial velocity and investigate saturation effects in the wings. Monitoring observations at high spectral resolution would place tighter constraints on the densities and distances of the absorbers.

REFERENCES

Arav, N., Korista, K.T., and de Kool, M. 2002, ApJ, 566, 699

Barvainis, R. 1987, ApJ, 320, 537

Bottorff, M.C., Korista, K.T., & Shlosman, I. 2000, ApJ, 537, 134

Brotherton, M.S., Green, R.F., Kriss, G.A., Oegerle, W., Kaiser, M.E., Zheng, W., & Hutchings, J.B. 2002, ApJ, 565, 800

Clavel, J., et al. 1991, ApJ, 366, 64

Collinge, M.J., et al. 2001, ApJ, 557, 2

Crenshaw, D.M., Boggess, A., & Wu, C.-C. 1993, ApJ, 416, L67

Crenshaw, D.M., & Kraemer, S.B. 1999, ApJ, 521, 572 (CK99)

Crenshaw, D.M., Kraemer, S.B., Boggess, A., Maran, S.P., Mushotzky, R.F., & Wu, C.-C. 1999, ApJ, 516, 750

Crenshaw, D.M., et al. 2000, AJ, 120, 1731

Crenshaw, D.M., et al. 2001, ApJ, 555, 633

Crenshaw, D.M., et al. 2002, ApJ, 566, 187

Ferland, G.J., et al. 1998, PASP, 110, 761

Gabel, J.R., et al. 2003, ApJ, 583, 178

George, I.M., Turner, T.J., Netzer, H., Nandra, K., Mushotzky, R.F., & Yaqoob, T. 1998, ApJS, 114, 73

Grevesse, N., & Anders, E. 1989, in Cosmic Abundances of Matter, ed. C.J. Waddington (New York: AIP), 1

Hamann, F., Barlow, T.A., Junkkarinen, V., & Burbidge, E. M. 1997, ApJ, 478, 78

Kaastra, J.S., et al. 2000, A&A, 354, L83

Kaastra, J.S., Steenbrugge, K.C., Raasen, A.J.J, van der Meer, R.L.J., Brinkman, A.C., Liedahl, D.A., Behar, E., & de Rosa, A. 2002, A&A, 386, 427

Kaspi, S., et al. 2000, ApJ, 535, L17

Kaspi, S., et al. 2002, ApJ, 574, 643

Korista, K.T., et al. 1995, ApJS, 97, 285

Kraemer, S.B. & Crenshaw, D.M. ApJ, 532, 256

Kraemer, S.B., Crenshaw, D.M., Peterson, B.M., and Filippenko, A.V. 1998, ApJ, 499, 719

Kraemer, S.B., et al. 2002, ApJ, 577, 98

Kraemer, S.B., et al. 2003, ApJ, 582, 125

Kriss, G.A., et al. 2000, ApJ, 538, L17

Krolik, J.H., & Kriss, G.A. 1995, ApJ, 447, 512

Lindler, D. 1998, CALSTIS Reference Guide (CALSTIS Version 5.1)

Maeder, A., & Meynet, G. 1989, A&A, 210, 155

Mathur, S., Elvis, M., & Wilkes, B.J. 1999, ApJ, 519, 605

Netzer, H., et al. 2002, ApJ, 571, 256

Reynolds, C.S. 1997, MNRAS, 286, 513

Ruiz, J.R., Crenshaw, D.M., Kraemer, S.B., Bower, G.A., Gull, T.R., Hutchings, J.B., Kaiser, M.E., & Weistrop, D. 2001, AJ, 122, 2961

Salpeter, E.E. 1977, ARA&A, 17, 73

Savage, B.D., Sembach, K.R., & Lu, L. 1997, AJ, 113, 2158

Shull, J.M., & van Steenberg, M.E. 1982, ApJS, 48, 95

Shull, J.M., & Van Steenberg, M.E. 1985, ApJ, 294, 599

Snow, T.P, & Witt, A.N. 1996, ApJ, 468, L68

Vrtilek, J.M., & Carleton, N.P. 1985, ApJ, 294, 106

Yaqoob, T., et al. 2003, ApJ, 582, 105

Fig. 1.— Far-UV continuum light curve of NGC 5548. Fluxes (10^{-14} ergs s^{-1} cm^{-2} Å^{-1}) at 1360 Å are plotted as a function of Julian date. The symbols are as follows: pluses – *IUE*, X's – FOS, triangle – *HUT*, squares – GHRS, diamonds - STIS. Vertical lines indicate the error bars ($\pm$ one sigma).

Fig. 2.— Spectra of the C IV region in NGC 5548 at three different epochs – 1996 (GHRS), 1998 (STIS) and 2002 (STIS). The UV absorption components are numbered for both members of the doublet: C IV λ 1548.2 and C IV λ 1550.8. Dotted lines give the zero flux level for each spectrum.

Fig. 3.— Portions of the STIS echelle spectra of NGC 5548, showing the intrinsic absorption lines in different ions. Fluxes are plotted as a function of the radial velocity (of the strongest member, for the doublets), relative to an emission-line redshift of z = 0.01676. The kinematic components are identified for the strong members of the doublets, and vertical dotted lines are plotted at their approximate positions. Strong Galactic absorption lines are labeled with "G". Fits to the NLR profiles are plotted as dashed lines.

Fig. 4.— Normalized *FUSE* spectra of the O VI doublet, plotted as a function of the radial velocity, relative to an emission-line redshift of z = 0.01676. The O VI λ1031.9 components are plotted in blue, and the O VI λ1037.6 components are plotted in red.

Fig. 5.— Spectral energy distribution of the input continuum used for the photoionization models.

Table 1. *HST* High-Resolution Spectra of NGC 5548

Instrument	Grating	Coverage (Å)	Resolution ($\lambda/\Delta\lambda$)	Exposure (sec)	Date (UT)
STIS	E140M	1150 – 1730	46,000	7639	2002 January 22
STIS	E230M	1607 – 2366	30,000	2700	2002 January 22
STIS	E140M	1150 – 1730	46,000	7639	2002 January 23
STIS	E230M	2274 – 3119	30,000	2700	2002 January 23
STIS	E140M	1150 – 1730	46,000	4750	1998 March 11
STIS	E230M	1607 – 2366	30,000	2295	1998 March 11
STIS	E230M	2274 – 3119	30,000	1905	1998 March 11
GHRS	G160M	1554[a] – 1590	20,000	13,600	1996 August 24
GHRS	G160M	1232[b] – 1269	20,000	4607	1996 February 17

Table 2. Low-Resolution FUV Spectra of NGC 5548

Instrument/ Grating	Coverage (Å)	Resolution ($\lambda/\Delta\lambda$)	Date (UT)
IUE SWP	1150 – 1978	~250	1978 June 27 – 1995 May 15[a]
FOS G130H	1150 – 1605	~1200	1992 July 5
FOS G130H	1150 – 1605	~1200	1993 February 3
FOS G130H	1150 – 1605	~1200	1993 April 19 – May 27[b]
HUT	820 – 1840	~450	1995 March 14

[a]Covers the C IV region.

[b]Covers the Lyα and N V region.

[a]See the IUE Merged Log at http://archive.stsci.edu/iue.

[b]See Korista et al 1995.

Table 3.   Absorption Components in NGC 5548

Comp.	Velocity[a] (km s^{-1})	FWHM (km s^{-1})	C_{los}[b]
1	−1041 (±11)	222 (±18)	>0.65
2	−667 (±4)	43 (±4)	0.77 (±0.03)
3	−530 (±19)	159 (±27)	0.70 (±0.02)
4	−336 (±4)	145 (±4)	0.92 (±0.02)
5	−166 (±6)	61 (±13)	>0.69
6	+78 (±6)	68 (±10)	>0.20

[a]Velocity centroid for a systemic redshift of z = 0.01676.

[b]Covering factor in the line of sight.

Table 4. Measured Ionic Column Densities $(10^{14} \text{ cm}^{-2})^a$

Comp.	Ion	GHRS[b]	STIS 1998	STIS 2002
1	H I	—	>1.34	>2.31
	N V	1.98 (0.29)	0.44 (0.18)	2.76 (0.10)
	C IV	0.11 (0.04)	<0.17	1.12 (0.12)
	Si IV	—	<0.10	<0.06
2	H I	>0.76	>0.61	>1.18
	N V	0.90 (0.11)	1.11 (0.16)	1.45 (0.13)
	C IV	0.39 (0.04)	0.51 (0.07)	0.56 (0.03)
	Si IV	—	<0.10	<0.06
3	H I	>1.79	>2.01	>1.65
	N V	7.40 (0.51)	3.04 (0.16)	8.64 (0.56)
	C IV	0.79 (0.23)	0.45 (0.11)	0.94 (0.26)
	Si IV	—	<0.10	<0.06
4	H I	>3.30	>2.97	>3.64
	N V	7.41 (0.87)	10.23 (0.79)	7.26 (0.78)
	C IV	3.43 (0.35)	3.44 (0.47)	2.70 (0.23)
	Si IV	—	<0.10	<0.06
5	H I	>0.77	>0.66	>0.92
	N V	1.05 (0.23)	1.18 (0.24)	1.45 (0.10)
	C IV	0.41 (0.18)	0.31 (0.13)	0.58 (0.05)
	Si IV	—	<0.10	<0.06
6	H I	0.13 (0.04)	0.13 (0.04)	0.13 (0.03)

[a]Based on C_{los} values in Table 3 for components 2, 3 and 4 and $C_{los} = 1$ for components 1, 5, and 6. Uncertainties are given in parentheses. "—" indicates not in wavelength coverage.

[b]GHRS C IV is not simultaneous with GHRS N V and H I.

Table 5.   Photoionization Models – STIS 2002

Comp.	N_H (cm^{-2})	U
1 "solar"	3.3×10^{19}	0.18
1 "2xN"	3.3×10^{18}	0.03
1 "dusty"	7.0×10^{18}	0.03
2 "solar"	2.1×10^{19}	0.21
2 "2xN"	1.7×10^{18}	0.03
2 "dusty"	3.8×10^{18}	0.03
3 "solar"	1.1×10^{22}	1.24
3 "2xN"	6.6×10^{19}	0.22
3 "dusty"	2.0×10^{20}	0.24
4 "solar"	1.1×10^{20}	0.21
4 "2xN"	8.7×10^{18}	0.03
4 "dusty"	1.9×10^{19}	0.03
5 "solar"	1.9×10^{19}	0.19
5 "2xN"	1.9×10^{18}	0.03
5 "dusty"	3.7×10^{18}	0.03

Table 6.   Predicted Ionic Column Densities $(10^{14}~\mathrm{cm}^{-2})^a$ –STIS 2002

Component	H I	N V	C IV	O VI	C VI	O VII	O VIII
1 "solar"	6.27	2.83	1.12	47.9	5.43	140	19.3
1 "2xN"	5.25	2.72	1.09	5.34	0.64	2.01	0.03
1 "dusty"	9.66	2.79	1.09	9.05	0.89	3.96	0.07
	(9.41)	(2.76)	(1.12)	(7.55)			
2 "solar"	3.36	1.45	0.53	26.7	35.9	92.6	15.7
2 "2xN"	2.74	1.42	0.57	2.79	0.37	1.05	0.01
2 "dusty"	5.06	1.50	0.57	5.03	0.50	2.28	0.04
	(3.25)	(1.45)	(0.56)	(3.15)			
3 "solar"	100	8.68	0.98	486.0	1.0e04	2.1e04	3.6e04
3 "2xN"	10.1	8.61	0.99	80.8	74.0	293.4	51.9
3 "dusty"	23.7	8.63	0.94	140	130	680	160
	(16.02)	(8.64)	(0.94)	(>10.0)			
4 "solar"	16.9	7.39	2.71	140	460	460	76.7
4 "2xN"	13.1	7.21	2.71	15.2	1.89	6.13	0.11
4 "dusty"	23.9	7.25	2.70	25.0	2.53	11.7	0.24
	(20.39)	(7.26)	(2.70)	(16.92)			
5 "solar"	3.39	1.50	0.57	26.4	31.4	130	12.5
5 "2xN"	2.83	1.47	0.58	2.87	0.35	1.09	0.02
5 "dusty"	5.11	1.47	0.58	4.78	0.47	2.10	0.04
	(5.60)	(1.45)	(0.58)	(3.69)			

[a]Measured values are in parentheses. The values for H I and O VI are from Brotherton et al. (2002).

Table 7. Predicted Ionic Column Densities $(10^{14}$ cm$^{-2})^a$ – STIS 1998

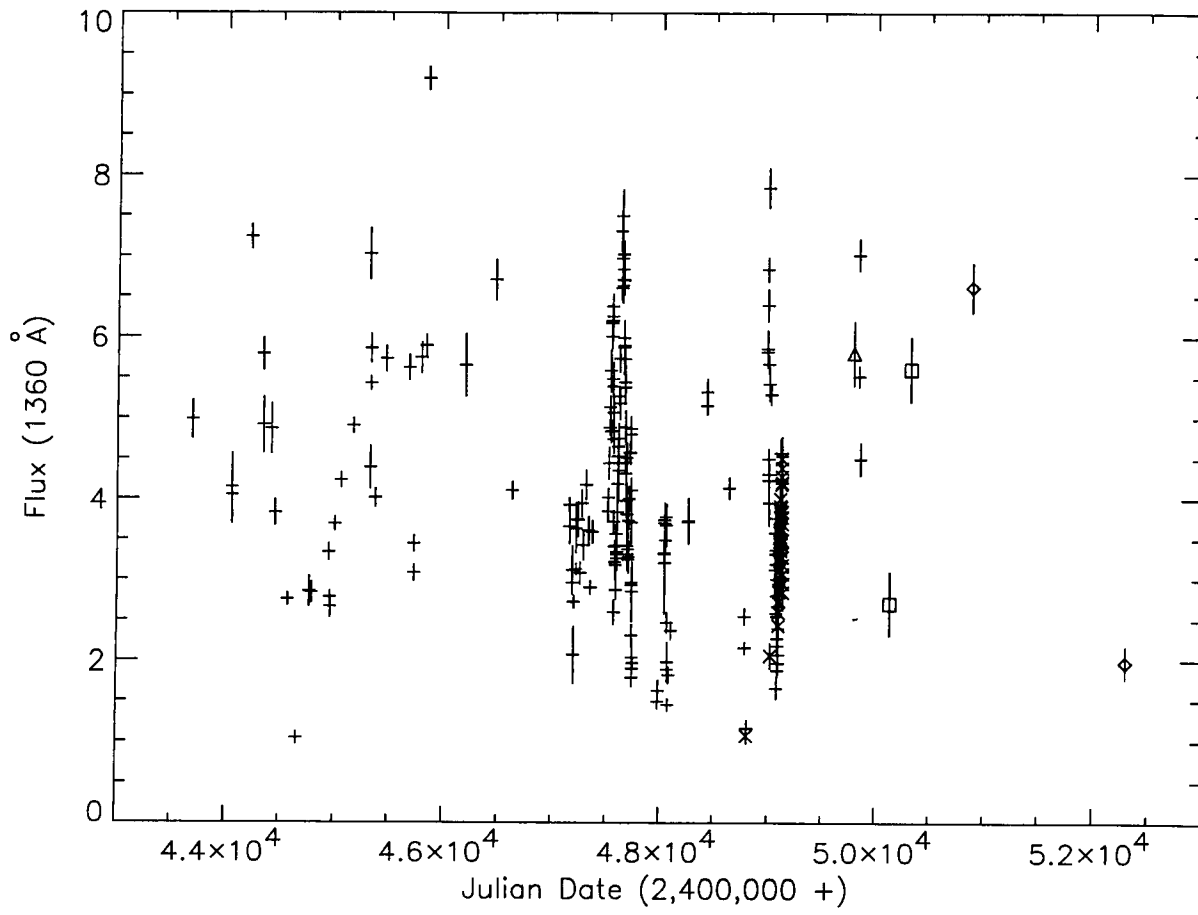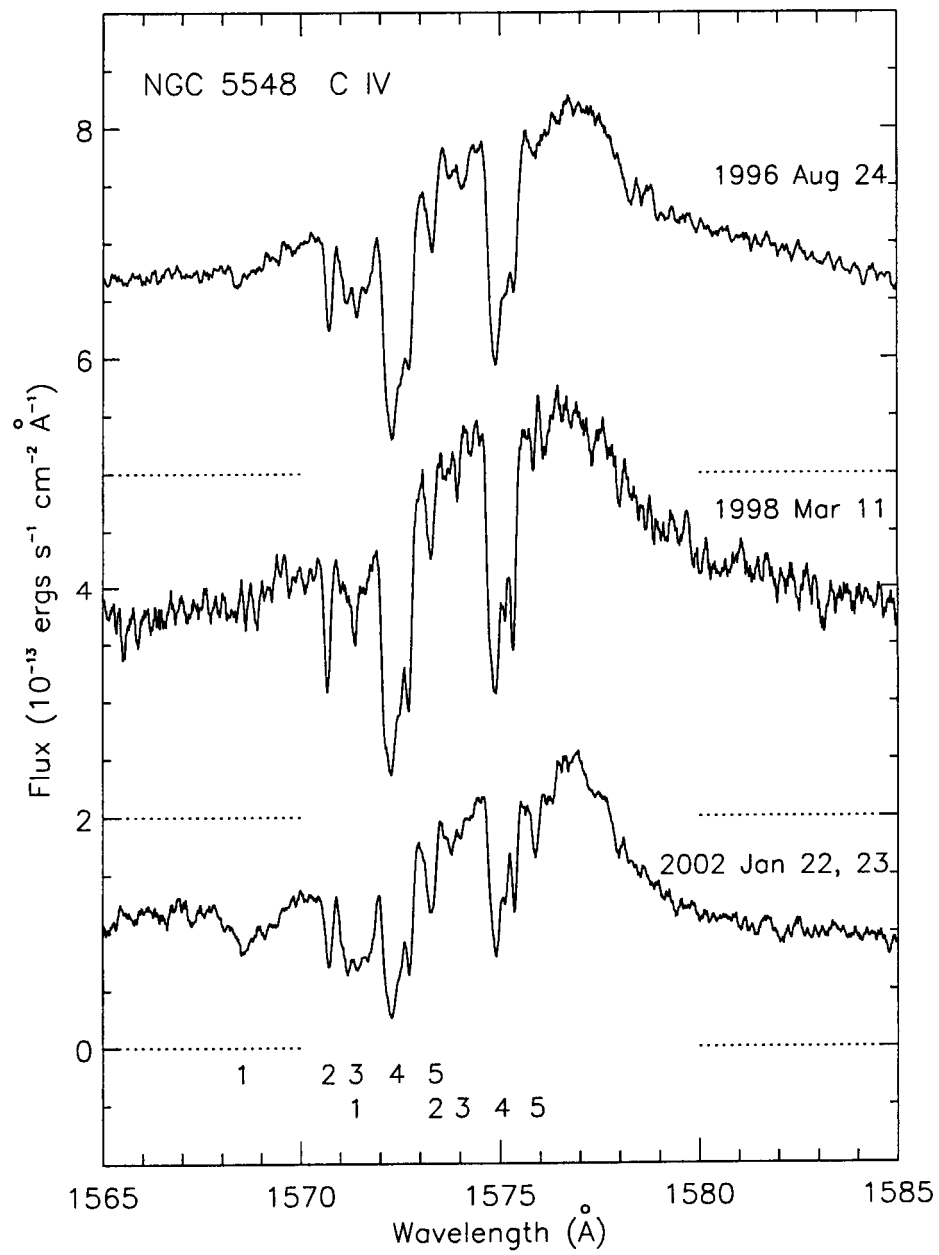| Component	U	N_H (cm^{-2})	H I	N V	C IV
2 "2xN"	0.03	1.4 x 10^{18}	2.26	1.17	0.47
2 "dusty"	0.03	2.9 x 10^{18}	3.87	1.15	0.44
			(>0.61)	(1.11)	(0.51)
3 "2xN"	0.22	2.5 x 10^{19}	3.82	3.25	0.37
3 "dusty"	0.24	7.8 x 10^{19}	8.61	3.30	0.35
			(>2.01)	(3.04)	(0.38)
4 "2xN"	0.03	1.2 x 10^{19}	18.32	10.2	3.83
4 "dusty"	0.03	2.6 x 10^{19}	33.7	10.2	3.82
			(>2.97)	(10.2)	(3.44)
5 "2xN"	0.03	1.3 x 10^{18}	2.02	1.05	0.41
5 "dusty"	0.03	2.8 x 10^{18}	3.87	1.12	0.44
			(>0.66)	(1.18)	(0.31)

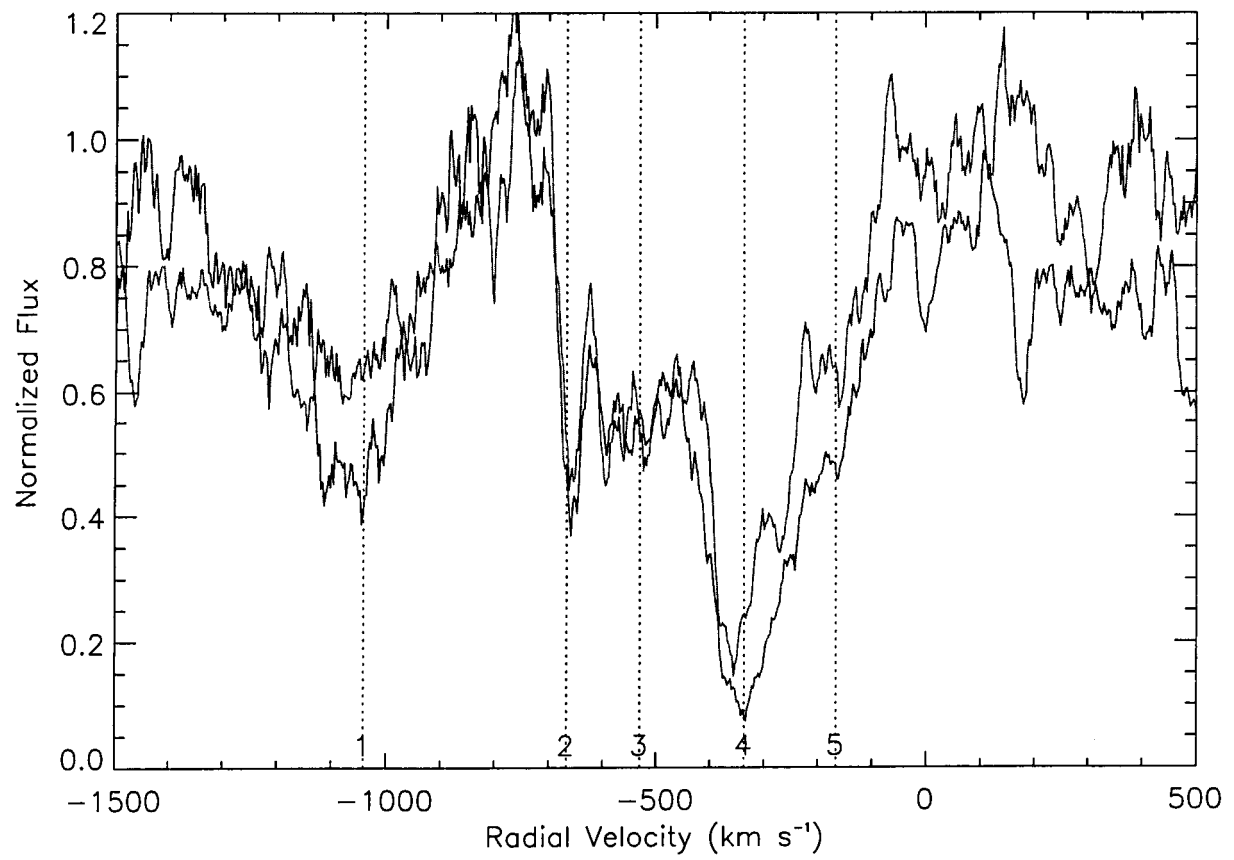^{a}Measured values are in parentheses.

Fig. 1.

Fig. 2.

Fig. 3.

Fig. 4.

Fig. 5.